

# Thermal Cycling Behavior of Quasi-Columnar YSZ Coatings Deposited by PS-PVD

Jiasheng Yang<sup>1,2</sup> · Huayu Zhao<sup>1</sup> · Xinghua Zhong<sup>1</sup> · Fang Shao<sup>1</sup> · Chenguang Liu<sup>1</sup> · Yin Zhuang<sup>1</sup> · Jinxing Ni<sup>1</sup> · Shunyan Tao<sup>1</sup>

Submitted: 29 May 2016/in revised form: 28 August 2016/Published online: 5 December 2016  
© ASM International 2016

**Abstract** Columnar-structured thermal barrier coatings, owing to their high strain tolerance, are expected for their potential possibilities to substantially extend turbine lives and improve engine efficiencies. In this paper, plasma spray-physical vapor deposition (PS-PVD) process was used to deposit yttria partially stabilized zirconia (YSZ) coatings with quasi-columnar structures. Thermal cyclic tests on burner rigs and thermal shock tests by heating and water-quenching method were involved to evaluate the thermal cycling and thermal shock behaviors of such kind of structured thermal barrier coatings (TBCs). Evolution of the microstructures, phase composition, residual stresses and failure behaviors of quasi-columnar YSZ coatings before and after the thermal tests was investigated. The quasi-columnar coating obtained had an average life of around 623 cycles when the spallation area reached about 10% of the total coating surface during burner rig tests with the coating surface temperature of  $\sim 1250$  °C. Failure of the coating is mainly due to the break and pull-out of center columnar segments.

**Keywords** plasma spray-physical vapor deposition (PS-PVD) · quasi-columnar structure · thermal barrier coating · thermal cyclic test · thermal shock test

## Introduction

Thermal barrier coating (TBC) systems are widely used in stationary turbines of power plants and aircraft turbines to improve the performance and efficiency of the engine (Ref 1, 2). A typical TBC system consists of an yttria partially stabilized zirconia (YSZ) topcoat, an intermediate thermally grown oxide (TGO) scale, a metallic bondcoat and a superalloy substrate (Ref 3, 4). The main properties and long-term stability of the individual TBC components are deeply depend not only on their chemical composition but also on their morphological feature. The latter can vary greatly with fabricate process. Currently, atmospheric plasma spraying (APS) and electron beam-physical vapor deposition (EB-PVD) are the two main processes used for TBC deposition, which results in very different microstructures of the coatings. An APS coatings built up of solidified droplets and produce lamellar-like splat morphology, whereas in EB-PVD, the materials condensates from the vapor phase and produces feather-like column structures (Ref 5-8). The result is that APS TBCs have lower manufacturing costs and a lower thermal conductivity, whereas EB-PVD TBCs have a higher strain tolerance.

A new spray process is called plasma spray-physical vapor deposition (PS-PVD) (Ref 9-17), which was primarily named as low-pressure plasma spraying-thin film process (LPPS-TF), enables vaporization of the injected spraying powder to a large extent and production of EB-PVD-like structures. These morphological characteristics

---

This article is an invited paper selected from presentations at the 2016 International Thermal Spray Conference, held May 10-12, 2016, in Shanghai, P.R. China, and has been expanded from the original presentation.

---

✉ Shunyan Tao  
sytao@mail.sic.ac.cn

<sup>1</sup> Key Laboratory of Inorganic Coating Materials CAS, Shanghai Institute of Ceramics, Chinese Academy of Sciences, CAS, Shanghai 201899, China

<sup>2</sup> University of Chinese Academy of Sciences, Beijing 100039, China

combine the low costs of a plasma spray process with the superior strain tolerance of column structures. Improved efficiency of the vacuum pumps in PS-PVD devices leads to pressures between 50 and 200 Pa in the working chamber (Ref 10, 11). Because of the lower pressure during the process, the plasma plume expands to a length reach over 2 m, and to 200–400 mm in diameter. Therefore, the plasma jet footprint covers the sample and allows coating of regions which are not in the line of sight of the plasma torch (“non-line of sight” coating). Although the pressure in the PS-PVD process is higher than that in the conventional PVD process, a high plasma jet temperature enables fine powder evaporation in the plasma plume, and the morphology of the coatings depends on the deposition parameters (Ref 13–15, 17). Additionally, it also allows formation of the unique microstructures and enables coating of complex substrate geometries. It has been shown by Detlev Stöver et al. that different kinds of YSZ coating microstructures depending on the application, including dense coatings, PVD-like columnar coatings and nano-sized solid clusters columnar coatings (quasi-columnar), could be applied by PS-PVD process through adjusting the spraying parameters (Ref 9, 10). Thereby, this relatively new technique can fill the gap between traditional thermal spray and EB-PVD processes.

In this paper, thermal cyclic tests on burner rigs and thermal shock tests by heating and water-quenching method were involved to evaluate the thermal cycling and thermal shock behaviors of such kind of PS-PVD quasi-columnar-structured YSZ coatings. Evaluation of the microstructures, phase composition, residual stresses and failure behaviors of the coatings before and after thermal tests was investigated.

## Experimental Procedures

### Coating Preparation

Ni-based superalloy (GH3128, Beijing CISRI-GAONA Materials & Technology Co., Ltd., China) was used as substrates, which were plate shape with a dimension of 25 mm × 25 mm × 2.7 mm and disk shape with a diameter of 30 mm and a thickness of 5 mm. Before the spraying processes, the substrate was sand-blasted using alumina powder and then followed by ultrasonically cleaning in ethanol. About 100- $\mu\text{m}$ -thick CoNiCrAlY bond coat was deposited by vacuum plasma spraying (VPS) (VPS/LPPS-PVD/CVD hybrid system, Oerlikon Metco, Wohlen, Switzerland).

All ceramic coatings were fabricated by a PS-PVD system (Oerlikon Metco, Wohlen, Switzerland). To achieve the low working pressure of 10–100 Pa and a

power input of 180 kW, the chamber was equipped with a vacuum pump unit consisting of a high suction capacity blower and two sets of pump stands, including screw pump and roots pump, and power sources. Since the standard F4-VB plasma torch cannot be operated at such higher power, the O3CP torch was applied which generates a supersonic DC plasma jet. The samples presented here were sprayed with a power input of 110–150 kW and a plasma gas flow of 95–120 slpm (using helium and argon as well as helium argon and hydrogen) at 100–150 Pa chamber pressure.

The feedstock material used for the coatings was an agglomerated 7 wt.% yttria partially stabilized zirconia powder (7YSZ) produced by Oerlikon Metco (Switzerland) designated as Metco 6700 and the grain size distribution with  $d_{10} = 2 \mu\text{m}$ ,  $d_{50} = 8 \mu\text{m}$ , and  $d_{90} = 18 \mu\text{m}$ , respectively. This agglomerated powder consisted of submicron  $\text{ZrO}_2$  particles and nano-sized  $\text{Y}_2\text{O}_3$  particles. Prior to spraying, the substrate was preheated by the plasma jet and the temperature was controlled by sweep movements of the plasma jet over the substrate. Before the deposition of the TBCs, the surface of the bondcoats was polished to be smooth with surface roughness Ra about 0.2  $\mu\text{m}$ . The improvement of lifetime by a decreased roughness has been observed to apply for PS-PVD coatings (Ref 10). During preheating and the coating deposition process, feeding additional oxygen into the vacuum chamber was used to obtain a dense TGO scale and prevent a loss of oxygen due to the high temperatures in the plasma plume (up to 15,000 K) in combination with the low oxygen pressure plasma plume, respectively.

### Thermal Shock and Cycling Test

The thermal shock test of the PS-PVD coatings was performed by heating and the water-quenching method. The plate shape samples were heated at an evaluated temperature of 1100 °C in a tube furnace (SLG 1400-60, Shanghai Shengli Test Instruments Co., Ltd., China) for 20 min and then followed by directly water quenching to room temperature. Before being placed into the furnace once again, the coating samples were dried by compressed air. Thermal cycling tests of the disk shape samples were performed in a flame shock facility (Shanghai Institute of Ceramics, Chinese Academy of Sciences, Shanghai, China). The coatings were heated for 3 min at  $1250 \pm 15$  °C. During the heating stage, the backside of the samples was cooled by compressed air to maintain a temperature gradient through the coatings thickness. During the cooling stage, the samples were cooled by compressed air from both sides for 3 min to below 200 °C. When visible spallation of the coating reached about 10% of the total coating surface, the thermal cycling test was stopped and the number of the cycles was defined as the lifetime of the TBCs.

## Coating Characterization

The phase composition of the as-sprayed coating was characterized by x-ray diffractometer (XRD, D/max 2550 V, Rigaku Industrial Corporation, Japan) with filtered Cu K $\alpha$  (40 kV, 40 mA) radiation at a scan rate of 4°/min in the 2 $\theta$  range of 20°–80°. The microstructures of the samples were examined using a scanning electron microscopy (SEM, TM3000, HITACHI, Japan) operated in backscattered electron image mode.

## Raman Spectroscopy and Cr<sup>3+</sup> Photoluminescence Piezo-Spectroscopy (PLPS)

The micro-Raman spectroscopy technique and PLPS method were used to measure the residual stresses distribution in the YSZ ceramic topcoat and the TGO scale, respectively (Ref 18–21). The measurements were made at room temperature in ambient air using 532 nm laser excitation in a confocal Raman microprobe (Renishaw Invia Confocal micro-Raman Microscope, Gloucestershire, UK). The diameter and spatial resolution of the laser beam at the specimen surface were about 1 and 3  $\mu\text{m}$ , respectively. Resolution of a spectrometer in the spectroscopic wavenumber range used (100–800  $\text{cm}^{-1}$ ) was less than 0.2  $\text{cm}^{-1}$ . It was well known that Raman shifts toward higher wavenumbers corresponding to an increase in the in-plane compressive residual stresses, and vice versa. The frequency shift could be converted into a biaxial stress depending on the relation for a bi-axially stressed stabilized tetragonal ZrO<sub>2</sub>.

$$\Delta\nu_{\text{TBC}} = \Pi_{\text{TBC}}\sigma_{\text{TBC}} \quad (\text{Eq 1})$$

where  $\Delta\nu$  referred to the frequency shift ( $\text{cm}^{-1}$ ) from the stress-free state,  $\sigma_{\text{TBC}}$  was the residual stress in the topcoat,

$\Pi_{\text{TBC}}$  was the piezo-spectroscopic coefficient, and the coefficient for plasma-sprayed TBC was reported to be 25  $\text{cm}^{-1} \text{GPa}^{-1}$  (Ref 19).

The PLPS method was used to measure stress in the TGO through the topcoat layer non-destructively. Resolution of a spectrometer in the spectroscopic wavenumber range used (14,300–14,500  $\text{cm}^{-1}$ ) was less than 0.2  $\text{cm}^{-1}$ , which gave the measured stress resolution of  $\sim 40$  MPa. The frequency shift of the luminescence in the TGO layer could be converted to the residual stress by the following expression:

$$\Delta\nu_{\text{TGO}} = \Pi_{\text{TGO}}\sigma_{\text{TGO}} \quad (\text{Eq 2})$$

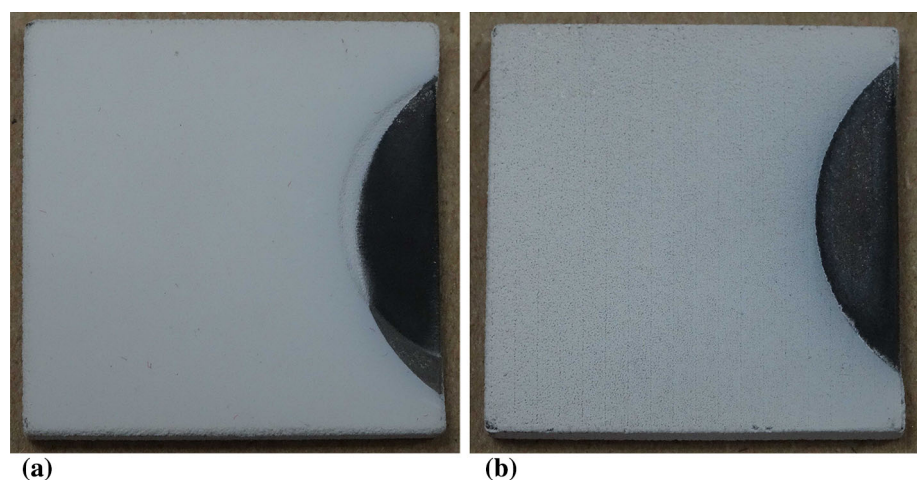
where  $\Pi_{\text{TGO}}$  was the piezo-spectroscopic coefficient and for plasma-sprayed TBC was set to be 5.07  $\text{cm}^{-1} \text{GPa}^{-1}$  (Ref 21).

## Results and Discussion

### Morphology of the As-Sprayed Coatings

The photographs of a PS-PVD coating are exhibited in Fig. 1. The difference between the front-side and back-side of the PS-PVD coating was that the former had a CoNiCrAlY bond coat, while the latter was not. The thickness of the YSZ topcoat on the back-side of the superalloy substrate was thinner than that on the front-side. An overview of the microstructure of a specimen, the typical characteristic structure of PS-PVD coatings with its feather-like columns, is shown in Fig. 2. At the bottom of the YSZ topcoat, initial columns with widths of few  $\mu\text{m}$  were deposited which make the coating look very dense. During the further deposition, some columns grew faster than the others and the slower growing

**Fig. 1** Front-side (a) and back-side (b) photographs of the PS-PVD coating



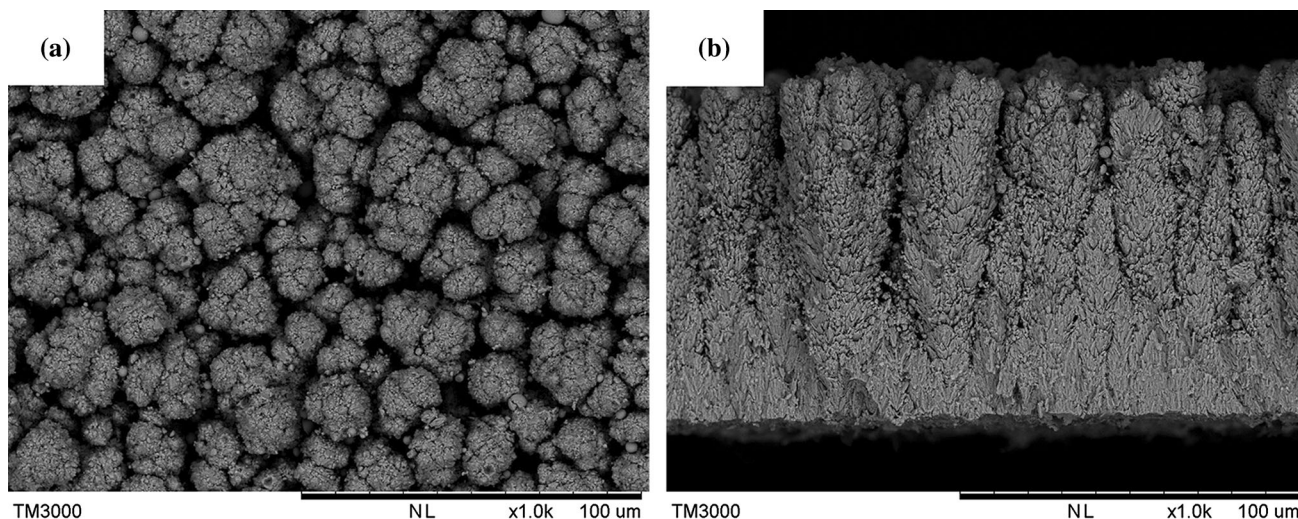


Fig. 2 Surface (a) and fracture surface (b) SEM micrographs of YSZ topcoat

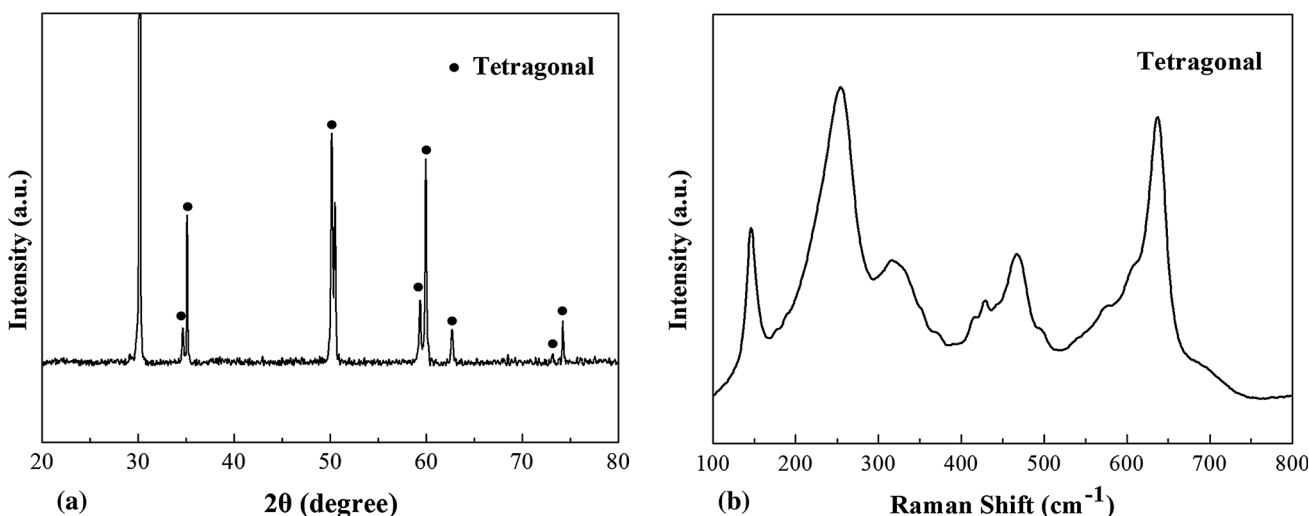


Fig. 3 XRD patterns (a) and Raman spectra (b) of as-sprayed coating

columns stopped. Thereby the feather-like columns structure which lead to the increased tolerance to strain were formed.

The XRD patterns and Raman spectra of as-sprayed coating are given in Fig. 3. The XRD patterns show that the coatings consist of non-transformable tetragonal phase. The micro-Raman spectroscopy was a powerful technique to study the structure changes in the coatings. Figure 3(b) gives micro-Raman spectra of the topcoat. The typical Raman bands for the tetragonal phase of yttria stabilized zirconia coatings were 148, 260, 320, 470, 612 and 640 cm<sup>-1</sup>, respectively. No monoclinic bands (at about 182 and 191 cm<sup>-1</sup>) were observed which confirmed the results obtained by XRD.

### Thermal Cycling Behavior of PS-PVD Coatings

Photographs of YSZ TBCs (here Φ30 mm × 5.8 mm substrate was used) before and after thermal cycling test are presented in Fig. 4. Apparent spot spallations were mainly occurred at the center of the YSZ topcoat surface of the sample. With the thermal cycling going on, the spalled area enlarged. After 623 cycles, the spallation area reached to ~10% of the total surface area of the specimen and thermal cycling test was stopped. Note that after thermal cycling, the column structure retains their original appearance and inter-columnar gaps were still exist, indicating that the YSZ coating had good sintering resistance, which is to say that the sintering of YSZ ceramic layer was



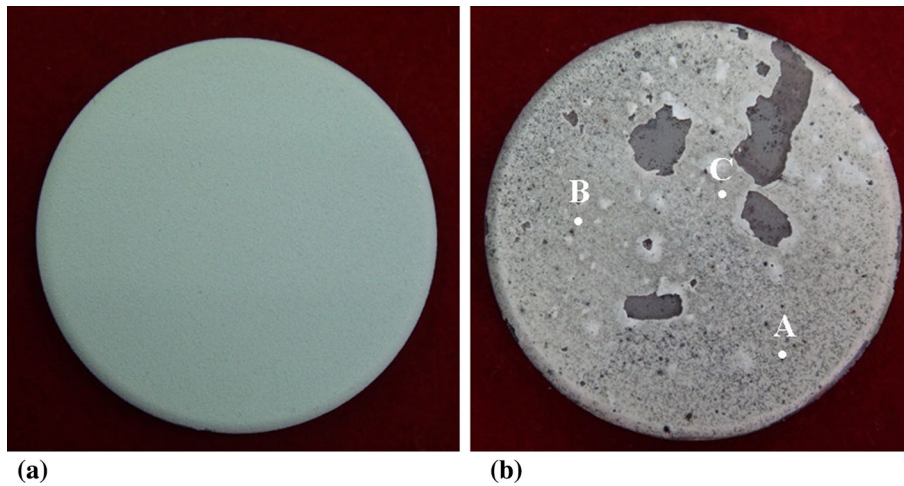


**Fig. 4** Photographs of YSZ TBCs before (a) and after thermal cycling 623 cycles (b)

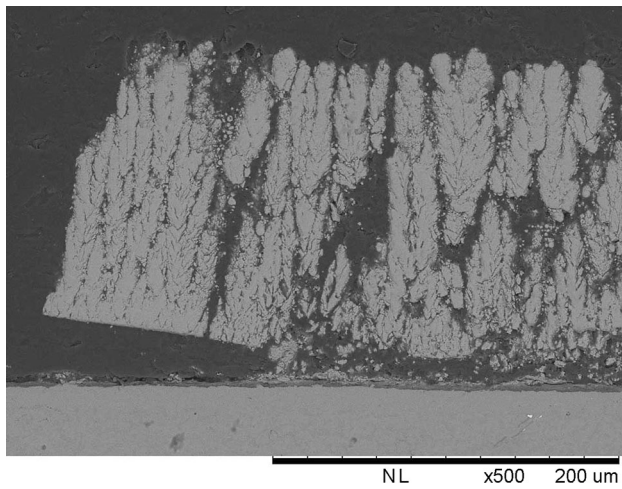


**Fig. 5** SEM micrograph of the cross section of PS-PVD coating after thermal cycling

not the major reason for leading to the spallation of the PS-PVD coatings, as shown in Fig. 5.

In order to have a better understanding of the failure mechanism, Figure 6 shows Raman spectra detected at three different locations on the specimen after thermal cycling test shown in Fig. 4(b). At the edge of the coating (position A), the spectra peaks correspond to vibrational modes of tetragonal zirconia, confirming the absence of monoclinic phase. However, at the center region of the coatings (position B and C), the phase transformation from tetragonal to monoclinic was indicated by the increase in intensity of the characteristic bands of monoclinic zirconia at 182 and 191  $\text{cm}^{-1}$ . The Raman spectra also illustrate another feature of the transformation to monoclinic, the volume fraction of the monoclinic phase could be quantified from the intensities of the tetragonal bands at 148 and

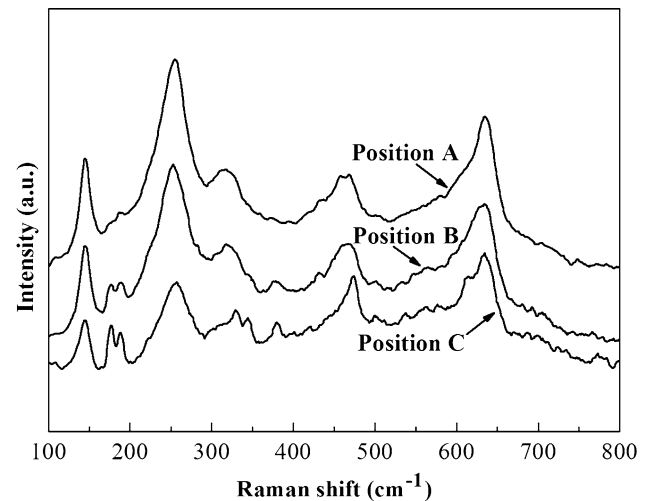


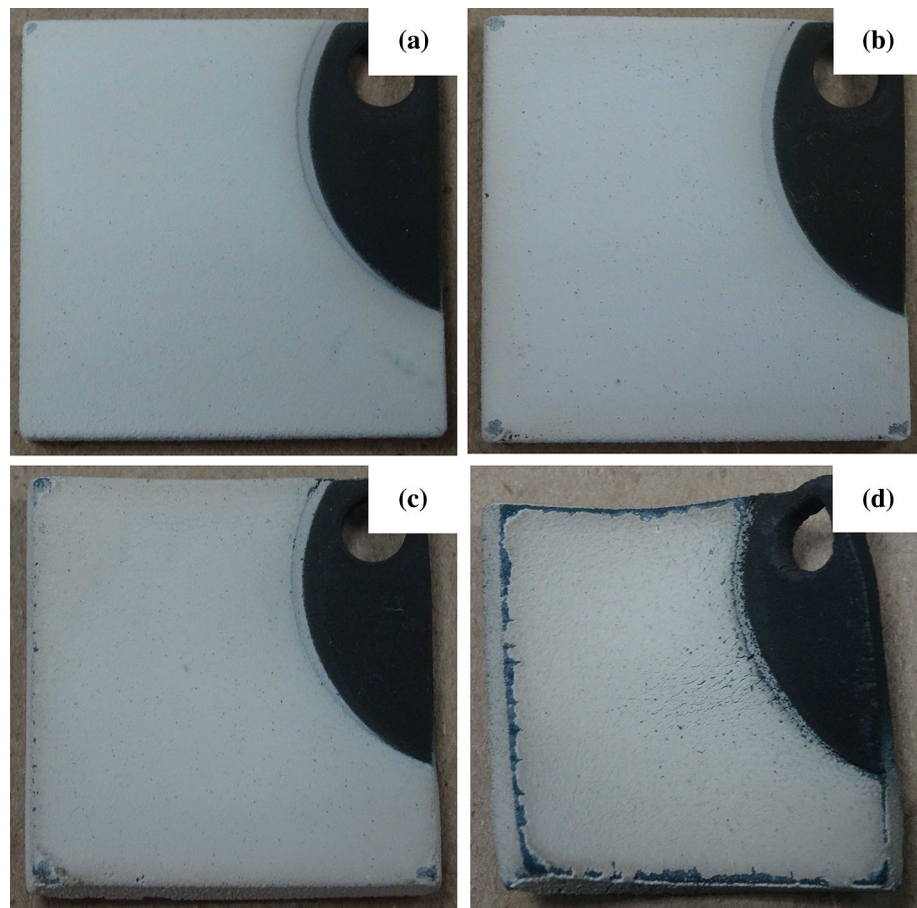
**Fig. 6** Raman spectra of different positions in PS-PVD coating after thermal cycling in Fig. 4(b)

263  $\text{cm}^{-1}$  and the monoclinic bands at 182 and 191  $\text{cm}^{-1}$ . Therefore, it was obvious that close to the center region (Position C) of the coatings had an increasing extent of phase transformation than relatively far away from the central area (Position B) during thermal cycling. It was well known that tetragonal-monoclinic phase transformation in 6–8 wt.% YSZ was accompanied essentially by a significant volume expansion of up to 5%, indicating that the phase transformation might be the reason for resulting in degradation and spallation of the PS-PVD coatings.

### Thermal Shock Behavior of PS-PVD Coatings

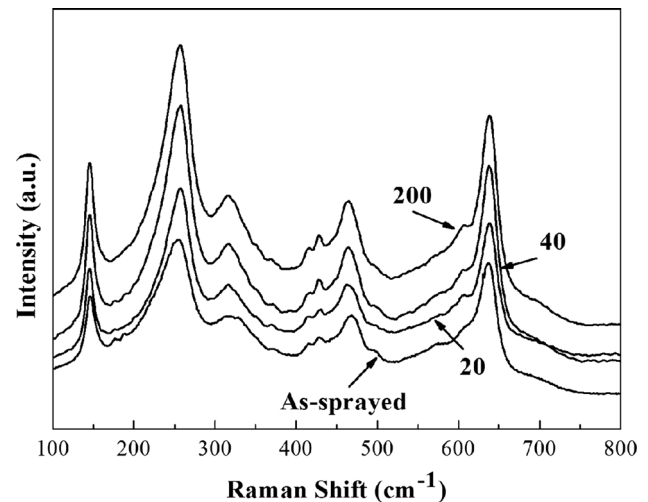
The thermal shock cycling and corresponding macroscopic surface micrographs of the PS-PVD YSZ sample by

**Fig. 7** Macroscopic images of PS-PVD samples during thermal shock tests (a) as-sprayed, (b) 20, (c) 70 and (d) 200 cycles



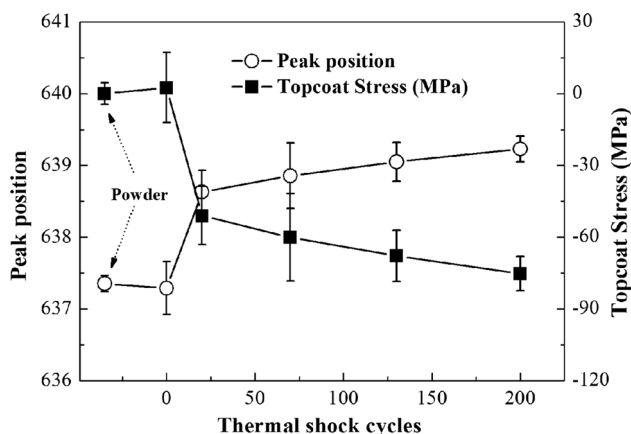
optimizing the process parameters are graphically presented in Fig. 7. As can be seen, the spallation of coatings samples started at the edges of the topcoat after 20 cycles, and then more edge spallation started associated with propagation to the adjacent areas on further cycling, and less than 5% spallation occurred even after 200 cycles. Obviously, the PS-PVD TBCs exhibit a significant improvement in the thermal shock resistance compared with the normal APS coatings. Lifetime extension of the PS-PVD coatings, as compared with the APS samples, can be attributed to the quasi-columnar structure. As the segmentation cracks can open during tensile loading in a manner similar to the EB-PVD coatings, reduction in thermal mismatch stress facilitated an improvement in the strain accommodation capability of the PS-PVD TBCs in the process of thermal shock.

Figure 8 gives the micro-Raman spectra of the topcoat before and after thermal shock test. No monoclinic bands ( $182$  and  $191\text{ cm}^{-1}$ ) were observed which confirmed that no phase transformation occurred. Raman scattering depends on electron-phonon interactions was very susceptible to local environments, thus it was also a



**Fig. 8** Raman spectra of as-sprayed coating and the coatings after different thermal shock cycles

suitable technique to investigate the changes in the residual stresses of ceramic topcoat. The principle Raman bands of zirconia tetragonal phase were at  $260$  and  $640\text{ cm}^{-1}$ , which



**Fig. 9** Variation of the residual stresses in the YSZ topcoat as a function of thermal shock cycles

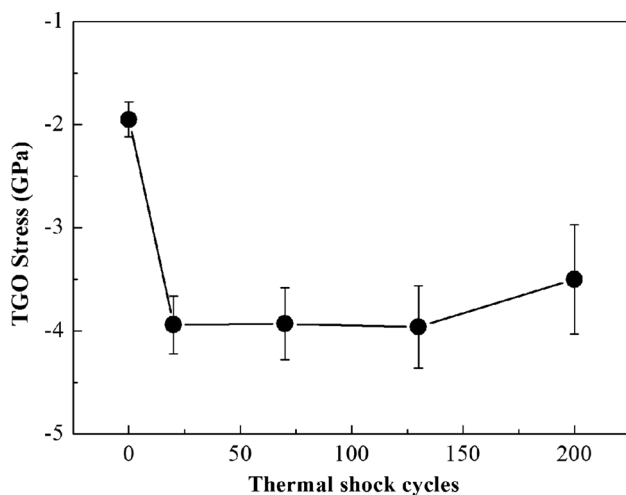


**Fig. 10** Average stresses measured from the ceramic topcoat surface in the TGO as a function of the thermal shock cycles

related with stretching modes of  $Zr-O_{II}$  and  $Zr-O_I$ . In previous Raman piezo-spectroscopy measurements distribution of residual stress in tetragonal-zirconia TBCs, the shift of the Raman peak at around  $640\text{ cm}^{-1}$  was used to measure stress distribution in the YSZ topcoat since it has a good signal-to-noise ratio (S/N). Considering the Raman band at about  $640\text{ cm}^{-1}$ , some shifts were observed due to the presence of different in-plane stress states (Ref 19).

Figure 9 represents the variation of position of the Raman peak at around  $640\text{ cm}^{-1}$  and the average residual stresses in the topcoat layer before and after thermal shock test. The Raman peak of the samples after thermal shock for 200 cycles shifted to a higher wavenumber ( $639.23 \pm 0.18\text{ cm}^{-1}$ ) compared with the as-sprayed one ( $637.28 \pm 0.36\text{ cm}^{-1}$ ) and the powder ( $637.35 \pm 0.11\text{ cm}^{-1}$ ). According to the formula (1), the conversion of Raman peak frequency shifts measured the in-plane residual stress

in the YSZ topcoat was gained. For the as-sprayed coatings, a low-level tensile stress ( $2.56 \pm 14.66\text{ MPa}$ ) was present in the topcoat. After thermal shock for 20 cycles, compressive stress was obtained. The average topcoat compressive stress was found to increase with thermal shock cycles, and the value was  $\sigma_{TBC} = -51.04 \pm 12.21$ ,  $-60.09 \pm 18.27$ ,  $-67.87 \pm 10.71$ ,  $-75.21 \pm 7.15\text{ MPa}$  for the 20, 70, 130 and 200 cycles of thermal shock test, respectively. The tensile stress developed in the as-sprayed coatings which was due to the lower cooling rate under a pressure of 100 to 200 Pa at the end of the spraying process. After thermal cycling, stress state has changed from tensile to compressive which was mainly due to the different coefficients of thermal expansion between the component of the TBC system ( $\alpha_{\text{Topcoat}} = 11 \sim 13 \times 10^{-6}/^{\circ}\text{C}$ ,  $\alpha_{\text{Bondcoat}} = 13 \sim 16 \times 10^{-6}/^{\circ}\text{C}$ ) (Ref 22). Attributed to stress relaxation in the ceramic topcoat at high temperature exposure, more compressive stress would accumulated when the coatings cooling from the high temperature to ambient temperature.

The distribution of residual stress in the TGO scale with various thermal shock cycles is given in Fig. 10. The measured in-plane stress through the topcoat surface (from  $-1.95 \pm 0.17$  to  $-3.96 \pm 0.40\text{ GPa}$ ) varied with the thermal shock cycles. At the beginning of thermal shock test, the measured in-plane TGO compressive stress firstly rapidly increased and then essentially maintain at a relatively stable value with further test. The value of compressive stresses reached to  $\sigma_{TGO} = -3.94 \pm 0.28$ ,  $-3.99 \pm 0.39$ ,  $-3.96 \pm 0.40\text{ GPa}$  for the 20, 70 and 130 cycles of thermal shock test, respectively. The apparently decreasing of the TGO stress was observed after 200 cycles, and the value was  $3.50 \pm 0.53\text{ GPa}$ . The decreased residual stress was mainly considered due to cracking generated in the topcoat layer or at interface between the topcoat and the TGO layer. Although spalling occurred at the edge and cracking was found in the center zone of the YSZ topcoat due to the obvious deformation of the nickel substrate during thermal shock test, the spallation area of the coating was less than 10% even after thermal shock for 200 cycles, given in Fig. 7(d). This shows that PS-PVD coating had excellent thermal shock resistance and the corresponding mechanism will be further investigate in the future work.

## Conclusions

In the present paper, quasi-columnar-structured thermal barrier coatings were fabricated by plasma spray-physical vapor deposition (PS-PVD) process. Microstructure, phase composition and residual stresses of the coatings before

and after thermal cycling and thermal shock test were investigated. Based on the experimental results, the following conclusions can be drawn:

- (1) The columnar-structured TBCs failed at the latest after 623 cycles during flame shock testing.
- (2) The as-sprayed quasi-columnar coatings consisted of tetragonal phase. Monoclinic phase was detected in the coatings after thermal cycling test especially nearby the spot spallation region.
- (3) The accumulated tensile stress in the as-sprayed ceramic topcoat changed to compressive state after thermal shock for 20 cycles, and then gradually increased. In addition, the compressive stresses in the TGO measured through the ceramic topcoat surface increased rapidly at first and then essentially maintain at a relatively stable value with further test.

**Acknowledgments** This work was jointly supported by the National natural Science Foundation (NSFC) under the Grant No. 51671208, Natural Science Foundation of Shanghai (No. 16ZR1440700) and Laboratory foundation of Chinese Academy of Sciences (Grant No. 16S084). And we also give our thanks to the special Project for Army-Civilian Combination of Shanghai Municipal Commission of Economy and Informatization (Grant No. JMJH2014053).

## References

1. S. Bose and J. DeMasi-Marcin, Thermal Barrier Coating Experience in Gas Turbine Engines at Pratt & Whitney, *J. Therm. Spray Technol.*, 1997, **6**(1), p 99-104
2. R.A. Miller, Thermal Barrier Coatings for Aircraft Engines: History and Directions, *J. Therm. Spray Technol.*, 1997, **6**(1), p 35-42
3. R. Vassen, A. Stuke, and D. Stöver, Recent Development in the Field of Thermal Barrier Coatings, *J. Therm. Spray Technol.*, 2009, **18**(2), p 181-186
4. D.R. Clarke and C.G. Levi, Materials Design for the Next Generation Thermal Barrier Coatings, *Annu. Rev. Mater. Res.*, 2003, **33**, p 383-417
5. T.R. Kakuda, A.M. Limarga, T.D. Bennett, and D.R. Clarke, Evolution of Thermal Properties of EB-PVD 7YSZ Thermal Barrier Coatings with Thermal Cycling, *Acta Mater.*, 2009, **57**, p 2583-2591
6. A. Cipitria, I.O. Golosnoy, and T.W. Clyne, A sintering Model for Plasma-Sprayed Zirconia TBCs. Part I: Free-Standing Coatings, *Acta Mater.*, 2009, **57**, p 980-992
7. A. Cipitria, I.O. Golosnoy, and T.W. Clyne, A Sintering Model for Plasma-Sprayed Zirconia TBCs. Part II: Coatings Bonded to a Rigid Substrate, *Acta Mater.*, 2009, **57**, p 993-1003
8. V. Lughì and D.R. Clarke, Low-Temperature Transformation Kinetics of Electron-Beam Deposited 5 wt.% Yttria-Stabilized Zirconia, *Acta Mater.*, 2007, **55**, p 2049-2055
9. A. Hospach, G. Mauer, R. Vaßen, and D. Stöver, Columnar-Structured Thermal Barrier Coatings (TBCs) by Thin Film Low-Pressure Plasma Spraying (LPPS-TF), *J. Therm. Spray Technol.*, 2011, **20**(1/2), p 116-120
10. A. Hospach, G. Mauer, R. Vaßen, and D. Stöver, Characteristics of Ceramic Coatings Made by Thin Film Low Pressure Plasma Spraying (LPPS-TF), *J. Therm. Spray Technol.*, 2011, **21**(3-4), p 435-440
11. S. Rezanka, G. Mauer, and R. Vaßen, Improved Thermal Cycling Durability of Thermal Barrier Coatings Manufactured by PS-PVD, *J. Therm. Spray Technol.*, 2012, **23**(1/2), p 182-189
12. G. Mauer, A. Hospach, and R. Vaßen, Process Development and Coating Characteristics of Plasma Spray-PVD, *Surf. Coat. Technol.*, 2013, **220**, p 219-224
13. G. Mauer, M.O. Jarligo, S. Rezanka, A. Hospach, and R. Vaßen, Novel Opportunities for Thermal Spray by PS-PVD, *Surf. Coat. Technol.*, 2015, **268**, p 52-57
14. K.V. Niessen, M. Gindrat, and A. Refke, Vapor Phase Deposition Using Plasma Spray-PVD, *J. Therm. Spray Technol.*, 2010, **19**(1/2), p 502-509
15. M. Goral, S. Kotowski, A. Nowotnik, M. Pytel, M. Drązewicz, and J. Sieniawski, PS-PVD Deposition of Thermal Barrier Coatings, *Surf. Coat. Technol.*, 2013, **237**, p 51-55
16. K.V. Niessen and M. Gindrat, Plasma Sprayed-PVD: A New Thermal Spray Process to Deposit Out of the Vapor Phase, *J. Therm. Spray Technol.*, 2011, **20**(4), p 736-743
17. L.H. Gao, H.B. Guo, L.L. Wei, C.Y. Li, and H.B. Xu, Microstructure, Thermal Conductivity and Thermal Cycling Behavior of Thermal Barrier Coatings Prepared by Plasma Spray Physical Vapor Deposition, *Surf. Coat. Technol.*, 2015, **276**, p 424-430
18. A.M. Limarga and R. Vaßen, Stress Distribution in Plasma-Sprayed Thermal Barrier Coatings Under Thermal Cycling in a Temperature Gradient, *J. Appl. Mech.*, 2011, **78**, p 011003-1-011003-1
19. M. Tanaka, M. Hasegawa, A.F. Dericioglu, and Y. Kawawa, Measurement of Residual Stress in Air Plasma-Sprayed Y<sub>2</sub>O<sub>3</sub>-ZrO<sub>2</sub> Thermal Barrier Coating System Using Micro-Raman Spectroscopy, *Mater. Sci. Eng., A*, 2006, **419**, p 262-268
20. R.J. Christensen, D.M. Lipkin, D.R. Clarke, and K. Murphy, Nondestructive Evaluation of the Oxidation Stresses Through Thermal Barrier Coatings Using Cr<sup>3+</sup> Piezospectroscopy, *Appl. Phys. Lett.*, 1996, **69**(24), p 3754-3756
21. K.W. Schlichting, K. Vaidyanathan, Y.H. Sohn, E.H. Jordan, M. Gell, and N.P. Padture, Application of Cr<sup>3+</sup> Photoluminescence Piezo-Spectroscopy to Plasma-Sprayed Thermal Barrier Coatings for Residual Stress Measurement, *Mater. Sci. Eng. A*, 2000, **291**, p 68-77
22. A. Rabiei and A.G. Evans, Failure Mechanisms Associated with the Thermally Grown Oxide in Plasma Sprayed Thermal Barrier Coatings, *Acta Mater.*, 2000, **48**, p 3963-3976